Heavy Ion, High-Energy, and Low-Energy Proton SEE Sensitivity of 90-nm RHBD SRAMs

E. H. Cannon, M. Cabanas-Holmen, *Member, IEEE*, J. Wert, T. Amort, R. Brees, *Member, IEEE*, J. Koehn, B. Meaker, and E. Normand, *Senior Member, IEEE*

***Abstract*—We measure the sensitivity of different 90-nm SRAM cells to single-event upsets (SEUs) caused by heavy ions, high energy protons, and low energy protons. We discuss radiation hardened by design techniques that impact SEU sensitivity.**

***Index Terms*—Direct ionization, proton radiation effects, radiation effects, single-event effects, single event upset.**

I. Introduction

RECENTLY, low energy proton testing has revealed direct proton sensitivity for some SRAM cells in ultra-deep submicron technologies [1]–[5]. In some cases, the charge liberated by a proton near its Bragg peak energy can directly upset an SRAM cell, despite the low linear energy transfer (LET) (less than 0.6 $\mathrm{MeV-cm^2/mg}$) of the protons. Higher energy protons indirectly upset SRAMs through interactions with nuclei which create higher LET reaction products capable of flipping an SRAM cell. Direct proton upset can have a much larger cross section than indirect proton upset, because the probability of nuclear interactions is so low. Since some space environments have a large flux of low energy protons, there is concern that low energy protons may be a significant source of single-event upsets (SEUs). Consequently, there is great interest in understanding this new radiation sensitivity.

We studied the SEE sensitivity of three SRAM bit cells fabricated in a commercial 90-nm process. Two SRAM cells use radiation hardened by design (RHBD) techniques to reduce low energy proton sensitivity, compared to a commercial cell. SRAM arrays designed using all 3 bit-cells incorporate additional RHBD techniques, such as error detection and correction (EDAC) and large bit spacing to reduce the rate of multiple-bit upset (MBU) that can defeat EDAC. We measured SEU sensitivity to heavy ions, high energy protons, and low energy protons. Experimental data demonstrate that in the 90-nm technology node, SRAM sensitivity to low energy protons is highly dependent on circuit design. Finally, we estimate the SEU rate from heavy ions, high energy protons, and low energy protons in different space environments. In summary, this paper analyzes SEU dependence on SRAM bit cell design at the 90-nm node, and it introduces a versatile technique to quickly estimate the low energy proton-induced SEU rate for a wide variety of missions.

Manuscript received July 16, 2010; revised September 08, 2010 and October 01, 2010; accepted October 06, 2010. Date of current version December 15, 2010. This work was supported in part by the DARPA under Contract HR0011-04-C-0106 and in part by the Defense Threat Reduction Agency under Contract HDTRA1-05-D-0001.

The authors are with the Boeing Company, Seattle, WA 98124 USA (e-mail: ethan.cannon@boeing.com).

Color versions of one or more of the figures in this paper are available online at http://ieeexplore.ieee.org.

Digital Object Identifier 10.1109/TNS.2010.2086482

II. SRAM Designs

We studied the SEU sensitivity of three distinct SRAM bit-cell designs: a commercial cell (Cell A), and two cells designed with varying RHBD techniques with different optimization goals. One RHBD cell (Cell B) was designed to maintain electrical performance with reduced SEU sensitivity, while the second RHBD cell (Cell C) was designed for maximal radiation hardness with electrical performance a lower priority.

Cell B uses the minimum RHBD techniques necessary to reduce SEU sensitivity, in order to achieve the best speed possible. The transistors were sized to augment the critical charge, Qcrit, to reduce the SEU contribution of direct upsets by low energy protons. The gate width of the pull-up and pull-down transistors was increased to enlarge Qcrit, and the gate width of the access transistors was increased to maintain cell stability. In addition, Cell B was designed according to logic design rules, in contrast to the commercial cell which takes advantage of compact spacing design rules available for SRAM. The drain and source area in Cell B grew in proportion with the gate width, but were not otherwise enlarged. Cell C employs more aggressive RHBD techniques resulting in complete immunity to direct proton upsets and multi-Mrad[Si] total ionizing dose performance [6]. In particular, the bit cell includes: 1) a guard band for latchup and field oxide leakage mitigation; 2) edgeless NMOS for transistor edge leakage mitigation; and 3) PMOS access transistors to remove the need for individual NMOS guard bands and to harden the bit lines to edge leakage effects. Multiple cell upsets in Cell C were studied in [7]. Table I shows that the improved radiation hardness of Cell C impacts the cell area, speed, and power more than the techniques used with Cell B. Additional RHBD techniques, such as using error detection and correction (EDAC), ensuring adequate bit spacing to minimize multiple-bit upsets and hardening circuits in the SRAM macro periphery are beyond the scope of this paper.

III. SEU Test Facilities

SEU tests on wirebonded samples were performed at the Lawrence Berkeley National Laboratory (LBNL) 88-inch cyclotron, the Indiana University Cyclotron Facility (IUCF), and the Boeing Radiation Effects Laboratory (BREL) Dynamitron. In all tests, the beam was incident on the chip topside. LBNL

TABLE I
SRAM CELL PARAMETERS, SCALED TO COMMERCIAL CELL

SRAM Bit Cell	Area	Setup+Access time	Power (1Kx72 array)
Commercial (Cell A)	1.0	1.0	1.0
High performance, high density RHBD cell (Cell B)	2.3	0.9	1.7
Multi-Mrad RHBD cell (Cell C)	3.6	1.8	2.5

TABLE II
IONS AND LET FOR HEAVY ION SEU TESTING AT LBNL

Ion	LET (MeV-cm^2/mg)
B	0.9
O	2.2
Ne	3.5
Ar	9.7
Cu	21
Kr	31
Xe	59

TABLE III
PROTON BEAM PROPERTIES

Facility	Beam Energy	Test Chamber	Method of control
IUCF	23-200 MeV	Open air	Degrader
LBNL	5-50 MeV	Open air	Degrader and tuning
BREL	1.0-2.0 MeV	Vacuum	Tuning

was the site of heavy ion tests on Cells A, B, and C. Normal incidence testing with the 10 MeV/nuclei cocktail was performed using the ions listed in Table II.

High energy proton testing of indirect proton upset was conducted at IUCF on all three cells, also at normal incidence. Direct upsets of Cells A and B by low energy protons were measured at the BREL Dynamitron; in addition, direct proton upsets of Cells A and C were measured at LBNL. Table III describes key properties of the proton beams used in the SEU test campaign. The low energy sensitivity of Cells A and C was tested at LBNL by tuning the beam to 12 MeV and degrading with sheets of aluminum foil to attain nominal beam energies as low as 5 MeV. Test time limitations did not permit retuning the LBNL cyclotron (predicted to require at least an hour per energy step, compared with a few minutes to change the degrader in air). The BREL Dynamitron provides a low energy beam ($\leq$2.5 MeV) with very little energy spread by tuning the beam in 100 keV steps.

The BREL Dynamitron is a continuous beam, high-voltage accelerator that utilizes a modified Cockroft-Walton voltage multiplier circuit driven by a high-power RF supply to generate the accelerating potential. The beam passes through the accelerator room floor into a 90° bending magnet that selects the energy and redirects the beam through the beam handling system to position it to impact test articles mounted in a cylindrical chamber, see Fig. 1. The beam handling system delivers electrons or protons with energy from 0.2 MeV up to 2.5 MeV into a 24-in-diameter evacuated scattering chamber equipped with a 10-in cryopump system, achieving a vacuum of better than 5×10^{-6} Torr (see Fig. 2). The beam energy is established

Fig. 1. Cut-away view of the BREL Dynamitron accelerator and beam handling system.

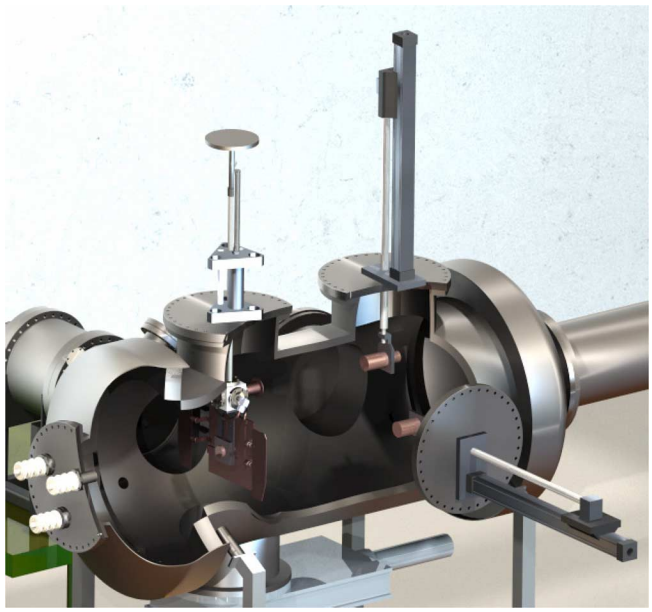

Fig. 2. Cut-away view of the BREL Dynamitron exposure chamber.

by varying the Dynamitron terminal voltage and the magnetic field in the bending magnet. The maximum beam current is approximately 10 mA. The beam is spread over the sample exposure area by means of a thin metal scattering foil mounted in the beamline; a 0.3 mil Al foil was used in the Cell A and Cell B SEU tests.

Beam dosimetry is performed using two Faraday cups: a "standard" cup which is the primary beam intensity standard, and a "monitor" cup which is used as a transfer calibration

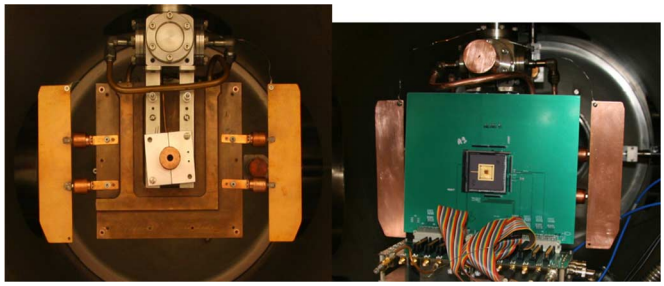

Fig. 3. Photograph of the standard Faraday cup on shaft (left) and Cell B test board and DUT (right).

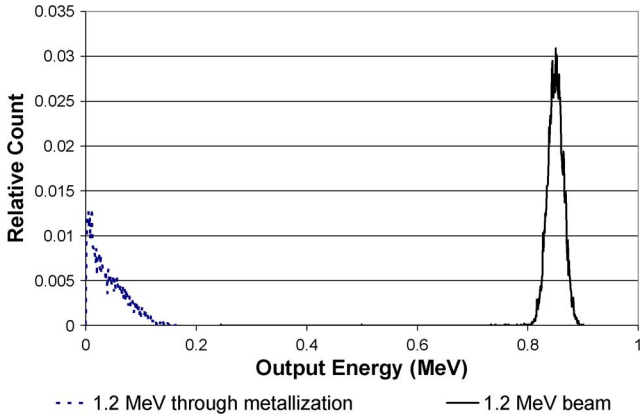

Fig. 4. Energy distribution of proton beam after passing through the scattering foil, simulated with SRIM-2008. The dotted curve shows the energy distribution of a 1.2 MeV proton beam after passing through the scattering foil and the chip metallization.

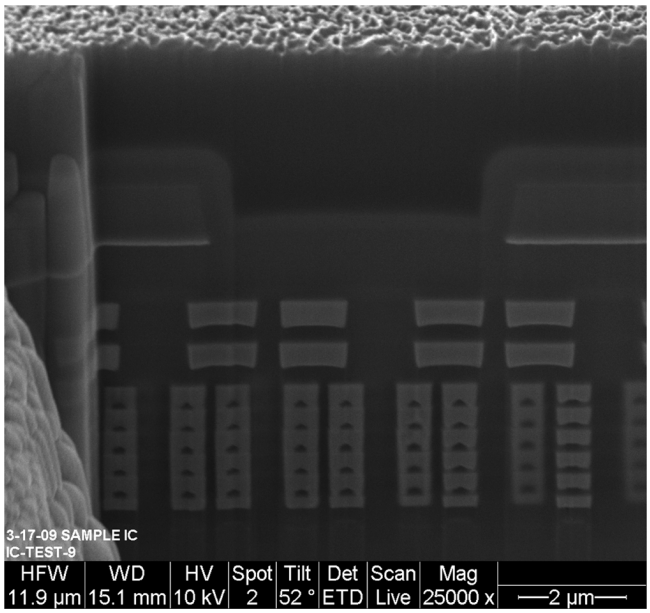

Fig. 5. FIB cross section of the 90-nm test chip.

standard. The standard Faraday cup is placed on a rotating vertical shaft that also the holds the test sample and associated test hardware. Fig. 3 shows the standard Faraday cup and the Cell B test board with a device under test (DUT). During calibration, the shaft places the standard cup directly in the beam to measure beam intensity at the DUT location. The monitor cup is located slightly below and well forward of the calibration cup to avoid blocking the beam, and monitors the off-axis beam flux. The current in each Faraday cup is measured with a Keithley 6517 A Electrometer. The calibration coefficient is the ratio of the standard cup current to the monitor cup current. During test, the DUT is rotated into to the beam, replacing the standard Faraday cup, and the monitor cup becomes a secondary standard. Beam flux at the sample plane is established by multiplying the current on the monitor Faraday cup by the calibration coefficient. The calibration process is repeated several times during the exposures and following each time the beam energy is retuned. Overall accuracy is expected to be better than $\pm 3\%$, considering the uncertainty in Faraday cup current measurements, aperture size, and run duration. Low energy protons can scatter off the monitor Faraday cup onto the DUT, introducing a small uncertainty in the beam energy spectrum. Scattered low energy protons would increase the SEU cross section for beam energies above the SEU peak, thus effectively broadening the peak of the SEU cross section versus energy curve towards higher energies. However, because the peak is well defined (no high energy tail in Fig. 7–Fig. 11 below), the data do not indicate this to be a significant issue.

The proton beam loses energy as it passes through the scattering foil. Not all protons lose the same amount of energy traversing the foil, introducing energy straggle. Fig. 4 presents the energy distribution of 10 000 1.2 MeV normal incidence protons simulated with SRIM-2008 [8]; the average proton energy at the DUT is 0.85 MeV. The beam has a tight distribution with 16 keV standard deviation. The thickness of the metallization layer was estimated from the focused ion beam (FIB) cross section of a test chip in Fig. 5. The metallization and passivation layers are modeled as a 4.9-μm-thick polyimide layer above an 8.9-μm-thick oxide layer in SRIM simulations to obtain the proton energy distribution at the active silicon, which is the dotted line at very low energy in Fig. 4. In the simulations, less than 60% of the incident 1.2 MeV protons reach the active silicon, and their average energy is 40 keV—very near the Bragg peak energy of 55 keV—with 32 keV standard deviation. This approximate treatment of the metallization as a uniform layer of dielectric material (the largest component, by volume) ignores the fact that different proton trajectories cross different materials, introducing additional spread in the final energy distribution; similar considerations have been discussed for alpha particle sensitivity in [9]. It is noteworthy that the DUT metallization and passivation layers significantly broaden the energy spectrum at the active silicon, despite the tight energy spread in the Dynamitron, especially near the Bragg peak where SRAMs are sensitive to direct proton upset. However, this energy broadening is an intrinsic characteristic of deep submicron integrated circuits, which have many metal wiring layers. The SRIM simulations compare reasonably well with the experimental data in Fig. 7, where no SEUs are observed for incident proton beam energy less than 1.0 MeV (corresponding to average proton energy at the DUT of 0.60 MeV). Given the limitations of the SRIM program, and the approximate representation of the metallization, only qualitative agreement with experiments is expected.

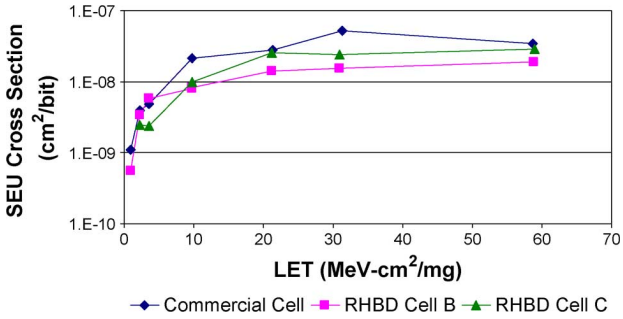

Fig. 6. Heavy ion SEU cross section at 0.9 V as a function of LET for all SRAM cell designs, measured at LBNL.

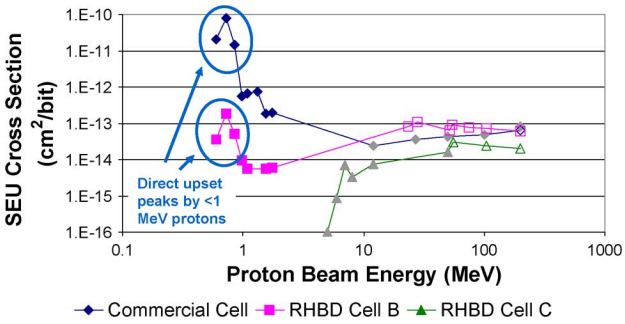

Fig. 7. Proton SEU cross section at 0.9 V as a function of proton beam energy for all SRAM cell designs. Open symbols represent IUCF data; light gray symbols represent LBNL proton data; dark solid symbols represent BREL data. Diamonds represent the commercial cell; squares represent Cell B; and triangles represent Cell C.

IV. SEU Test Data

Fig. 6 presents the total SEU cross section as a function of LET for the three SRAM cells. The three bit cells have similar heavy ion-induced SEU sensitivity. In particular, all cells have very low threshold LET, less than 1 $\mathrm{MeV}-\mathrm{cm}^2/\mathrm{mg}$. Cell A has the largest SEU cross section, and Cell B has the lowest cross section, but for most ions all cells match within a factor of 2 1/2. The saturation cross section depends on several factors—including sensitive node area, Qcrit, and the prevalence of multiple-cell upsets—making it difficult to predict accurately. The RHBD cells—Cells B and C—are designed to reduce low energy proton sensitivity; however, heavy ion sensitivity is mitigated with RHBD techniques in the array design, including, EDAC, bit spacing, and scrubbing.

Fig. 7 graphs the normal incidence total proton SEU cross section as a function of proton energy (average proton energy incident on the DUT) for the three SRAM cells: open symbols represent IUCF data; light gray symbols denote LBNL measurements; and BREL results are presented as closed symbols. The low energy peak is indicative of direct proton upsets [2]–[5]. The SEU cross section peak occurs at 0.7 MeV, well above the Bragg peak energy (55 keV), because of the energy loss in the metallization, as shown in Fig. 5. Cell A is very sensitive to direct proton upset, with a peak cross section three orders of magnitude above high energy proton cross section results. In fact, this peak cross section approaches the lowest heavy ion cross section measured at LBNL. For this cell, protons near the Bragg peak can liberate more than the critical charge in the sensitive volume, resulting in the cross section peak. In contrast, Cell B peaks at the same order of magnitude as the high energy cross section, almost four orders of magnitude below the lowest heavy ion cross section measurement at LBNL. The SEU cross section at 1.8 MeV is roughly an order of magnitude below the high energy cross section measured at IUCF, showing the decrease in sensitivity to indirect proton upset at low energies. Because of the augmented critical charge of Cell B, the typical proton at the Bragg peak cannot flip a bit; however, protons that liberate more charge than average (due, for example, to straggle in LET or interactions that result in a longer path length through the sensitive volume) cause upsets. Finally, Cell C does not exhibit a low energy cross section peak due to direct proton ionization, and the cross section values measured at IUCF exceed the LBNL proton results. Proton direct ionization cannot overcome the cell's large critical charge even with variations in charge deposition. In Fig. 7, Cell B has the largest SEU cross section above 20 MeV, and Cell C has the smallest SEU cross section at all energies.

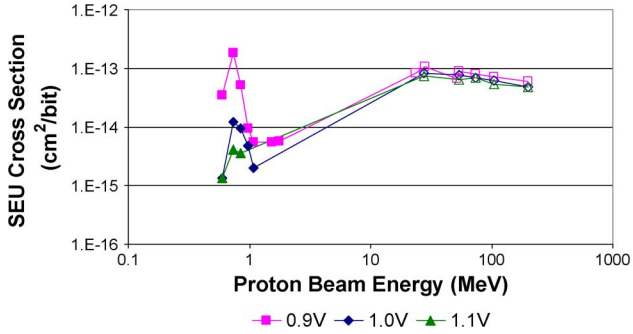

Fig. 8. Proton SEU cross section of Cell B as a function of proton beam energy and voltage. Open symbols represent IUCF data; solid symbols represent BREL data.

Fig. 8 presents the SEU cross section of Cell B as a function of proton energy for different voltages. The high energy IUCF data manifest little voltage dependence; in contrast, the magnitude of the low energy peak observed at BREL decreases an order of magnitude as the voltage is increased from 0.9 V to 1.0 V. Cell B is barely sensitive to low energy protons, as demonstrated by the small peak; hence, only a small voltage increase is sufficient to increase the critical charge above the level collected during low energy proton events and sharply reduce the low energy proton SEU cross section. On the other hand, Cell A—the commercial cell—is very sensitive to low energy protons. Accordingly, the low energy proton SEU cross section in Fig. 9 exhibits little voltage dependence. As the voltage is varied from 0.9 V to 1.0 V, the critical charge increases proportionally and the memory cells can withstand a few of the events that would cause upsets at the lower voltage. If the voltage were raised to the point where the critical charge was larger than the charge liberated by a typical proton at the Bragg peak, a large decrease in the SEU cross section would be expected, similar to the voltage dependence observed in [3].

Low energy proton testing was also performed at non-normal incidence. Figs. 10 and 11 plot the 0.9 V SEU cross section of Cell A and Cell B, respectively, at 0°, 30°, and 45° (Cell A only). At a larger angle of incidence, the proton beam has a

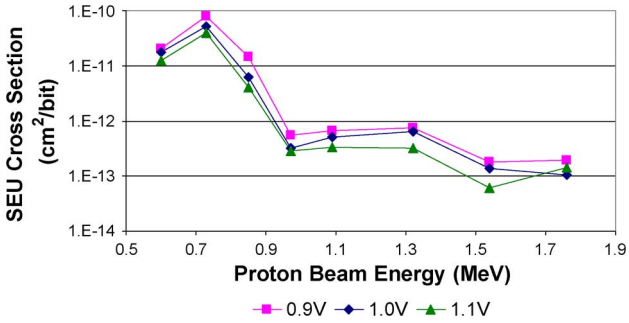

Fig. 9. BREL proton SEU cross section of Cell A as a function of proton beam energy and voltage.

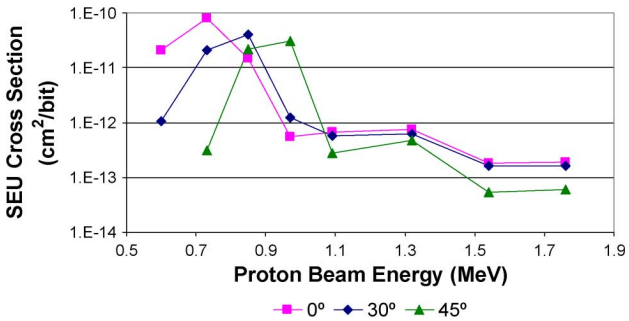

Fig. 10. BREL proton SEU cross section of Cell A at 0.9 V as a function of proton beam energy and an incident angle.

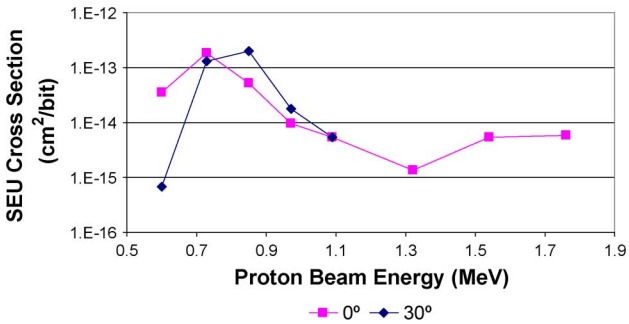

Fig. 11. BREL proton SEU cross section of Cell B at 0.9 V as a function of proton beam energy and incident angle.

longer path length through the DUT metallization, reducing the energy at the active silicon; consequently, the cross-section peak shifts to higher energy.

Various levels of SRAM sensitivity to direct proton upsets have been reported in different process technologies. SRAMs in the IBM 65-nm and 45-nm SOI processes have a direct proton upset peak four orders of magnitude above the high energy proton cross section [2], [3]; SRAMs in the TI 65-nm process peak 3–4 orders of magnitude above high–energy proton cross sections [4]. Lawrence reported startling results on a 90-nm SRAM that the low energy proton peak is 6–7 orders of magnitude above the high-energy proton cross section, equal to the cross section in a heavy ion beam with an LET of 40 $\mathrm{MeV-cm^2/mg}$ [5], [10]. These authors also tested an SRAM cell at the same process node that was not sensitive to direct proton upsets. The direct proton upset peak of the commercial cell in Fig. 9 is comparable to the 65-nm TI data, and significantly smaller than the 90-nm results in [5] and [10]. BREL tests reveal that the high-performance, high-density RHBD cell, Cell B, is barely sensitive to low-energy protons, with a low-energy proton peak cross section comparable to the high-energy proton cross section—the lowest direct proton upset peak reported to date. Finally, the multi-Mrad RHBD cell, Cell C, displays negligible low-energy proton sensitivity. These low-energy proton data demonstrate that direct proton upset sensitivity is strongly dependent on the bit cell, and can be mitigated by cell design.

No latchup events were detected at 1.2 V and 120 °C, when irradiated by the Xe beam at an angle of 60° (with an effective LET of 117 $\mathrm{MeV-cm^2/mg}$) for an effective fluence of at least 1×10^7 $\mathrm{ion/cm2}$. Thus, all SRAM cells are suitable for use with Boeing's 1.0 V 90-nm RHBD library without risk of single event latchup.

V. On-Orbit SEU Rate Prediction

In this section, we evaluate on-orbit SEU rates for all three SRAM cells, based on the measured heavy ion and proton sensitivity. The CREME96 tool estimates SEU rates from heavy ions and indirect proton upsets. It does not calculate proton direct upset rates accurately, because it assumes the proton has constant LET through the sensitive volume. This is not a good assumption for protons near their Bragg peak, where the LET changes over tenths of microns, while the 90-nm SRAMs have sensitive volume dimensions on the order of a micron.

We estimate the direct proton-induced SEU rate from the proton differential flux after shielding $d\Phi/dE$, calculated by the AP8 model in CREME96

$$\text{SEU rate} = \sigma_{\text{peak}} * \frac{d\Phi}{dE} * \Delta E * 4\pi \tag{1}$$

where σ_{peak} and ΔE are the maximum value and width (in MeV) of the low proton energy SEU cross section peak. We assume isotropic sensitivity to low energy protons, so (1) includes a factor of 4π steradians.

Table IV compares uncorrected and corrected SEU rates for the three SRAM cells in an 800 km polar orbit, with 100 mil Al shielding, for solar minimum and worst day flare environments. The uncorrected SEU rate is the rate of bit flips in the array, most of which are remedied by EDAC. The corrected error rate assumes single error correction, double error detection, with 32 data bits and 7 check bits, and a 1 h scrub interval at solar minimum (1 s scrub interval during the flare). It accounts for accumulating two SEU in a data word during a single scrub interval according to [7, Eq. 4], and for the solid angle for a heavy ion to strike two bits in the same data word. These arrays are designed so that the spacing of bits in a data word exceeds the range of low-energy protons and of secondary particles from high-energy protons, hence a single proton cannot upset two bits in data word. Heavy ion and indirect proton SEU rates were calculated with the CREME96 tool. The direct proton SEU rate was calculated from (1). The relative contributions of low-energy protons, high-energy protons, and heavy ions to the total uncorrected error rate for each SRAM cell are graphed in Fig. 12(a) and (b) for solar minimum and worst day environments, respectively. The direct proton SEU rate estimate has larger uncertainty than for the heavy ion and indirect proton SEU rates, which precludes

TABLE IV
UNCORRECTED AND CORRECTED BIT-ERROR RATE

		Uncorrected Error Rate (error/bit-day)				Corrected Error Rate (error/bit-day)
		Heavy Ion	Indirect Proton	Direct Proton	Total	
800 km, polar solar min	Cell A	6.2E-7	8.7E-7	3E-7	1.8E-6	1.7E-10
	Cell B	1.7E-7	1.6E-6	7E-10	1.8E-6	9.2E-11
	Cell C	2.4E-7	4.7E-7	0	7.1E-7	2.0E-11
800 km, polar worst day	Cell A	1.2E-3	5.1E-5	2E-4	1.4E-3	1.9E-7
	Cell B	1.6E-4	9.5E-5	4E-7	2.6E-4	1.7E-8
	Cell C	2.3E-4	3.2E-5	0	2.6E-4	7.8E-9

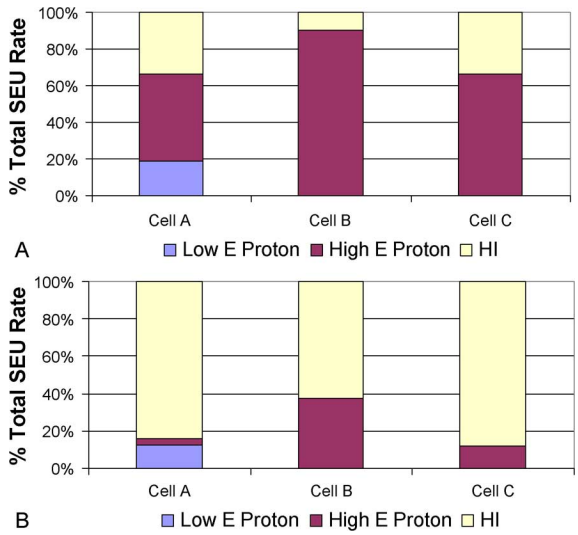

Fig. 12. Relative SEU contribution from low-energy protons, high-energy protons, and heavy ions for all SRAM cells in 800 km, polar orbit with 100-mil Al shielding for (a) the solar minimum environment and (b) worst day flare condition.

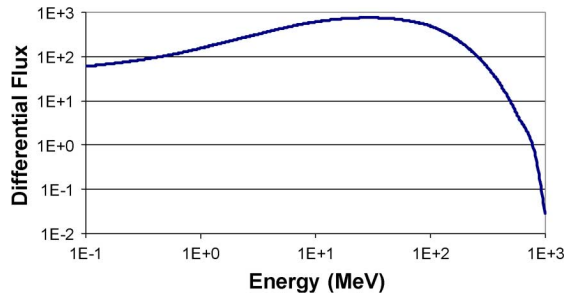

Fig. 13. Differential proton flux for 800 km, polar orbit at solar minimum with 100 mil Al shielding.

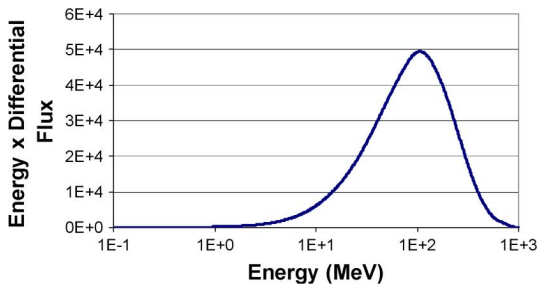

Fig. 14. Energy times differential proton flux for 800 km, polar orbit at solar minimum with 100 mil Al shielding. The integral flux in an energy region is proportional to the area under the curve. Most protons have energy greater than 10 MeV.

rigorous quantitative comparisons. Cell C has negligible sensitivity to low-energy protons. The direct proton upset rate calculated by (1) for Cell B is at least two orders of magnitude lower than the other SEU components, for both solar minimum and worst day flare environments. The RHBD techniques employed in Cell B mitigate the low-energy proton sensitivity, even considering large uncertainty in the low-energy proton upset rate. For Cell A, the commercial cell, the calculated direct proton upset rate is the same order of magnitude as the indirect proton upset rate both at solar minimum and in the worst day flare environment. Hence, low-energy proton sensitivity is expected to be a significant SEU source for Cell A in the environments evaluated. Similar patterns are observed in geosynchronous and international space station orbits (not shown in Table IV).

Fig. 13 plots the differential flux for the 800 km, polar orbit at solar minimum, with 100 mil Al shielding, as calculated by the AP8 model in CREME96. The differential flux peaks in the energy regime where indirect proton upset occurs; around 1 MeV, corresponding to the direct proton upset peak, the differential flux is significantly lower. Since the differential flux in Fig. 13 is defined per unit energy, the SEU rate is approximately proportional to the product of the differential flux, the SEU cross section, and the width of the cross-section peak. The direct proton upset peak in Fig. 7 is very narrow ($\sim$0.2 MeV), while the indirect proton upset peak is much broader, greater than 100 MeV. In this environment, the combination of higher flux and broader cross-section peak for the indirect proton upset mechanism compensate for the larger direct proton upset cross section of Cell A.

Fig. 14 plots the energy times the differential flux for the same environment as in Fig. 13. In Fig. 14, the integral flux in an energy range is proportional to the area under the curve; clearly, most incident protons are too energetic to cause direct proton upsets.

The goal of (1) is to provide an approach to quickly estimate low-energy proton SEU rates for a wide variety of missions.

This approach includes the effect of changing proton LET in the sensitive volume by starting with the measured SEU cross section $\sigma_{\rm peak}$, which is an improvement over the CREME96 tool. However, it also assumes constant SEU contributions from all angles, resulting in the 4π steradian factor. This isotropic angular sensitivity is based on the spherical shielding approximation, and it also assumes the area of the cross-section peak—represented by the product of the maximum value and the width of the low-proton energy SEU cross-section peak $\sigma_{\rm peak}$ and ΔE in (1)—does not change with angle. The spherical shell approximation enables a general evaluation of different possible radiation environments for multiple programs without requiring detailed knowledge of the potential satellite design. For a specific application, a more accurate analysis can include the actual distribution of shielding material [11]. Additional experiments with finer energy resolution at multiple angles are desirable to allow integration of the total SEU sensitivity in the low proton energy peak, for a better understanding of the angular sensitivity.

Other approaches to estimate the SEU rate from direct proton upsets exist in the literature. One approach is to calculate the ratio of the SEU rate due to low energy protons relative to the SEU rate due to high-energy protons [3], [10]. For the 800 km polar orbit at solar minimum, the integrated flux from 1 to 300 MeV is 3.6×10^3 times larger than the flux from 0.8 to 1.0 MeV; for Cell A, the direct proton upset peak cross section is three orders of magnitude larger than the maximum high-energy cross section. Consequently, the direct proton SEU rate is expected to be approximately 0.36 times the indirect proton upset rate, which agrees well with Table IV.

In [4], the authors perform SEU simulations of a 65-nm SRAM with the MRED tool. In [4, Fig. 8], the direct proton upset rate for the International Space Station orbit at solar minimum with 100 mil Al shielding is approximately 2×10^{-8} upset/bit-day. The peak cross section for this 65-nm SRAM is roughly 1×10^{-10} $\rm cm^2$/bit (see [4, Fig. 4]). Using the proton flux at 1 MeV computed by CREME96 and $\Delta E = 0.2$ MeV, (1) predicts the direct proton upset rate to be 8×10^{-8} upset/bit-day. This rate is $4\times$ larger than the MRED simulation results, which is an impressive agreement for these disparate-rate estimation methods. Finally, we note that [12] calculates SEU rates analytically assuming the critical charge Qcrit and sensitive volume dimensions are known. Ultimately, all direct proton SEU rate estimates need to be compared to on-orbit SEU data to establish their validity. In particular, we note that (1) has not been validated with on-orbit SEU data; thus, it should be used with caution while the uncertainties have not been quantified.

VI. Conclusion

We measured the SEE sensitivity of two RHBD 90-nm SRAM bit cells, and a commercial 90-nm SRAM bit cell. All three SRAM cells can be used with a 90-nm RHBD application-specific IC (ASIC) library. The SRAM cells are immune to SEL for an effective LET of 117 $\rm MeV-cm^2/mg$, even with extreme bias conditions 20% above nominal voltage. The different bit cells have similar heavy ion and high-energy proton sensitivity (measured cross sections within a factor of 4). The commercial SRAM cell is very sensitive to direct proton upsets, with a low energy cross-section peak three orders of magnitude larger than the high-energy cross-section. RHBD techniques successfully mitigated this sensitivity, as one RHBD cell did not show any low-energy proton sensitivity, and the other RHBD cell had a peak comparable to the high-energy proton cross section. We estimate the SEU rate from low-energy protons based on the measured cross section and the differential flux in multiple space environments, including flares. The estimated low-energy proton SEU rate can be a significant SEU contribution for the commercial cell. Thus, sensitivity to low energy protons is a concern for advanced complementary metal–oxide semiconductor (CMOS) processes, but RHBD techniques can mitigate this sensitivity with acceptable area, speed, and power impact. This paper analyzes SEU dependence on SRAM bit-cell design at the 90-nm node, and it introduces a versatile technique to quickly estimate the low-energy proton-induced SEU rate for a wide variety of missions.

Acknowledgment

The authors would like to recognize the contribution of F. Nelson, M. Baze, and B. Hughlock.

References

[1] K. P. Rodbell, D. F. Heidel, H. H. K. Tang, M. S. Gordon, P. Oldiges, and C. E. Murray, "Low-energy proton-induced single-event-upsets in 65 nm node, silicon-on-insulator latches and memory cells," *IEEE Trans. Nucl. Sci.*, vol. 54, no. 6, pp. 2474–2479, Dec. 2007.

[2] D. F. Heidel *et al.*, "Low energy proton single-event-upset test results on 65 nm SOI SRAM," *IEEE Trans. Nucl. Sci.*, vol. 55, no. 6, pp. 3394–3400, Dec. 2008.

[3] D. F. Heidel *et al.*, "Single-event upsets and multiple-bit upsets on a 45 nm SOI SRAM," *IEEE Trans. Nucl. Sci.*, vol. 56, no. 6, pp. 3499–3504, Dec. 2009.

[4] B. D. Sierawski *et al.*, "Impact of low-energy proton induced upsets on test methods and rate predictions," *IEEE Trans. Nucl. Sci.*, vol. 56, no. 6, pp. 3085–3092, Dec. 2009.

[5] R. K. Lawrence, J. F. Ross, N. F. Haddad, R. A. Reed, and D. R. Albrecht, "Soft error sensitivities in 90 nm bulk CMOS SRAMs," in *Proc. IEEE Rad. Effects Data Workshop*, 2009, pp. 123–126.

[6] M. Cabanas-Holmen, E. H. Cannon, T. Amort, R. Brees, A. Kleinosowski, and B. Meaker, "Optimizing electrical performance and TID hardness in high performance 90-nm RHBD SRAM Caches," presented at the NSREC, Denver, CO, Jul. 2010.

[7] D. G. Mavis, P. H. Eaton, M. D. Sibley, R. C. Lacoe, E. J. Smith, and K. A. Avery, *IEEE Trans. Nucl. Sci.*, vol. 55, no. 6, pp. 3288–3294, Dec. 2008.

[8] SRIM-The Stopping and Range of Ions in Matter. [Online]. Available: www.srim.org

[9] H. H. K. Tang, C. E. Murray, G. Fiorenza, K. P. Rodbell, and M. S. Gordon, "Importance of BEOL modeling in single event effect analysis," *IEEE Trans. Nucl. Sci.*, vol. 54, no. 6, pp. 2162–2167, Dec. 2007.

[10] R. K. Lawrence, J. F. Ross, N. F. Haddad, M. A. McMahan-Norris, R. A. Reed, and D. R. Albrecht, "Proton induced soft error sensitivities in 90 nm bulk CMOS," presented at the SEE Symp., La Jolla, CA, Apr. 2009.

[11] J. A. Pellish, M. A. Xapsos, R. L. Ladbury, C. A. Stauffer, T. M. Jordon, and T. R. Oldham, "Impact of spacecraft shielding on direct ionization soft error rates," presented at the NSREC, Denver, CO, Jul. 2010.

[12] L. D. Edmonds and K. J. Edmonds, "A method for estimating SEU rates from protons by direct ionization," *IEEE Trans. Nucl. Sci.*, vol. 55, no. 5, pp. 2666–2678, Oct. 2008.